Devices & Services Co.

D & S Technical Note 79-16*

THE SOLAR SPECTRUM REFLECTOMETER (SSR)

INTRODUCTION

Rapid, accurate, and repeatable measurements of solar reflectivity are possible with Devices and Services new Solar Spectrum Reflectometer (SSR). The unit, consisting of a measurement head and associated electronics, features a direct digital readout of total solar reflectivity with resolution to 0.001 and repeatability of +/- 0.003 reflectivity units. Drift compensation and automatic zeroing is designed to minimize the requirements for periodic calibration by the user, thus making the instrument ideal for quality control and R & D. Other features include the use of a single tungsten-hålogen light source, and a four detector combination that provides a measurement spectrum that closely approximates the air mass two solar spectrum. Other terrestrial solar spectra can be set by the user.

This technical note is concerned with the theory of the solar reflectivity measurement and with the operation of the reflectometer. The basic ideas are summarized below and are described in detail in later sections of this note.

1. Measurement Spectrum - The tungsten-halogen lamp and the Barium Sulfate reflectance paint on the sidewalls of the measurement head (Figure 6) provide a near diffuse light source at the sample port. Four filtered detectors located in the collimator measure reflected energy in different wavelength ranges. A weighted sum of the four detector outputs produce the air mass two solar measurement spectrum. How the individual measurement spectra for each detector-filter combination was determined and how these were combined to match the solar spectrum, is presented.

2. Effect of Incident Energy Distribution - the collimator views energy reflected by the sample at an angle of 20 degrees from the normal to the sample. If the incident energy is perfectly diffuse, this measurement is equivalent to the reflectivity of the surface for beam radiation at the same 20 degrees incidence angle. Some error will be introduced in the measurement if the incident energy reaching the sample is not perfectly diffuse. Data on the distribution of the energy exiting the port is presented.

*Several improvements have been made since 1979. In particular, the method for adjusting specular intensity and autozero circuit operation have been modified and documented in TN 82-1 and TN 83-1.

The errors are minimum for diffuse and specular surfaces and surfaces that show primarily diffuse and specular components (error is less than 2% of reflectivity). The maximum error occurs for the rare case where back scatter into the direction

of the incident beam is predominant. The worst case of back-scattering found in the literature is the data of Orlova [1]. Even in this unlikely situation, the error is less than 3% of reflectivity.

3. Incident Energy Control - The lamp current is controlled with a silicon cell which maintains the filament at a near constant temperature. This minimizes possible drift, both in the measurement spectra due to the change in relative spectral output with filament temperature, and drift in reflectivity reading due to the change in overall output of the lamp. In addition, the control of the lamp reduces the so called "substitution error", that is caused by the fact that a very small amount of the energy reflected by the sample striking the walls of the chamber is reflected back toward the sample, adding to the incident energy. Experimental data indicates that for the worst case the lamp control limits the substitution error to a maximum of 0.01 reflectivity units.

4. Instrument Operation - In normal operation, by simply placing a sample over the measurement port the reflectivity appears on the display. Only occasional servicing or calibration is required. For use in quality control or automatic controls, more information about the instrument operation is required. This section includes an operational schematic and a description of the instrument operation. Timing for the autozero feature, optional outputs, and stray light considerations are detailed.

SOLAR MEASUREMENT SPECTRUM

Rather than attempting to simulate the solar spectrum with the light source, an inexpensive tungsten halogen light source and a multiple detector filter system produce the solar measurement spectrum. The measurement spectrum results from the weighted sum of the response from four individual detectors adjusted to match the solar spectrum. Three filtered photovoltaic detectors are used for the ultraviolet to the near infrared portion of the spectrum, and a lead sulfide cell is used for the infrared out to 2.5 microns. Electronic compensation linearizes the lead sulfide output, and eliminates drift due to temperature and light history (see discussion of device operation).

The individual response spectra for the four filtered detectors are shown in Figure 2. For convenience they will be designated UV, Blue, Red, and IR, even though there is overlap in most cases.

Filter combinations for each photo-detector were chosen to shape the individual response spectrum, $R(\lambda)$, so that the resulting measurement spectrum is a close fit to the air mass two solar

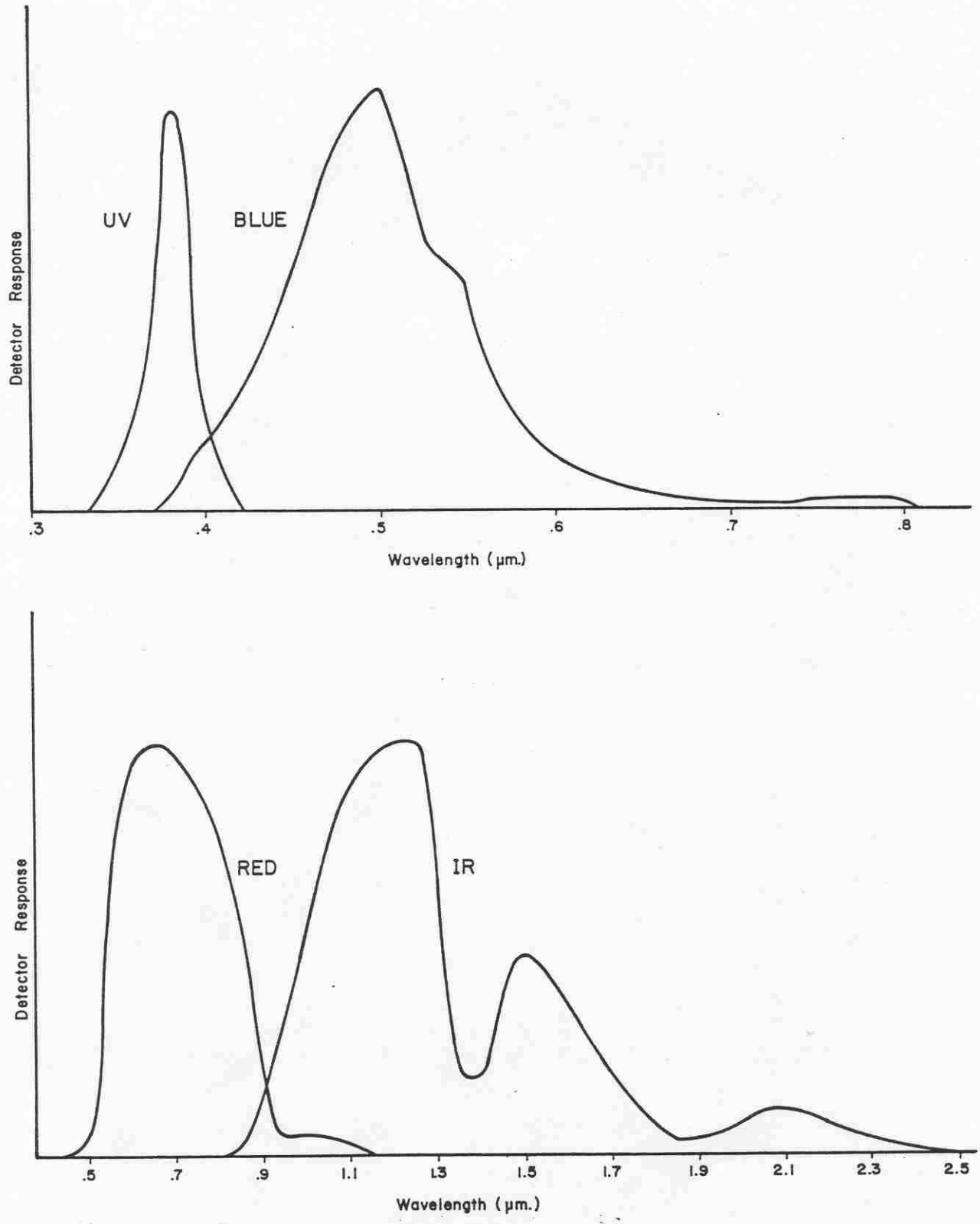

Figure 2. Response Spectra of Detectors

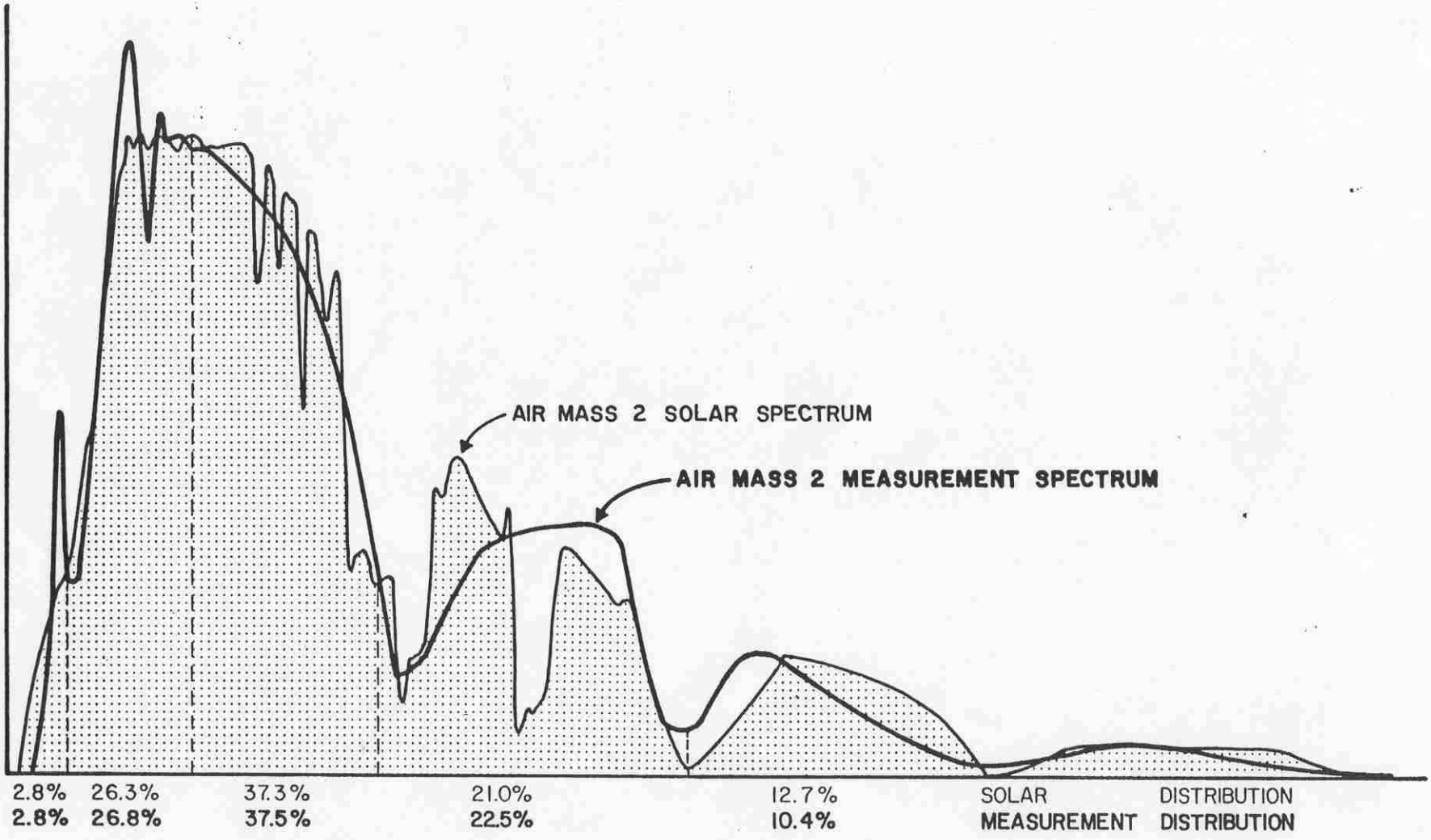

Figure 3. Comparison of the Air Mass 2 Solar Spectrum and the Air Mass 2 Measurement Spectrum

spectrum. Notice in particular, the two minima in the IR spectrum (Figure 2) that result from the thin water filter over the detector, and match the minima in the solar spectrum due to atmospheric absorption by water vapor and carbon dioxide.

The response spectrum depends on the spectral intensity of the source and the sensitivity of the detector filter combination.

$$R(\lambda) \propto I(\lambda)S(\lambda) \tag{1}$$

where $I(\lambda)$ is the spectral intensity distribution of the light source $S(\lambda)$ is the relative spectral sensitivity of the detector filter combination. (To avoid confusion, hereafter, the word detector is used to refer to one of the filtered detectors, UV, Blue, Red or IR). The method used to determine the $R(\lambda)$ for a given detector requires a set of filters calibrated for spectral transmissivity over the wavelength range encompassed by the detector. The transmissivity, τ, of each calibration filter is measured for the light source with the given detector. This transmissivity can be expressed as a function of the response spectrum $R(\lambda)$.

$$\tau_i = \frac{\int_\lambda R(\lambda)\tau_i(\lambda)d\lambda}{\int_\lambda R(\lambda)d\lambda} \tag{2}$$

With a number of filters it is possible to estimate $R(\lambda)$.

Ideally, a set of non-overlapping narrow band pass filters would establish $R(\lambda)$ with the least uncertainty. The filters used here exhibit the sharp cut-ons and cut-offs at different wavelengths to provide good resolution.

Spectral transmissivity measurements for all of the filters were made with a Beckman DK2A spectrophotometer. A set of 63 acetate color filters were calibrated from 0.3 to 0.96 microns. Water filters, clear plastics, glass IR filters and two narrow band filters were used for the IR out to 2.5 microns. To make the measurement of the transmissivity of each calibration filter for a detector light source combination, the collimator was removed from the measurement head and arranged to view the light exiting from the port with and without the filter in place. The response spectrum, $R(\lambda)$, was determined numerically using an iterative algorithm that begins with an initial guess for the response curve and corrects the curve to reduce the difference between the measured transmissivity values and the predicted value using Equation (2). The routine minimizes the sum of the square of the difference between the measured and predicted transmissivity for all of the filters.

The numbers of filters, the number of points on the response spectrum, and the integrating interval (wave length), are summarized in Table 1 for the four detectors. For all but the Blue detector, the response curve was assumed to be a straight line between points for the purpose of calculation. For the Blue detector enough filter data was available to consider the $R(\lambda)$ constant over each integration interval. The resulting response curves were smoothed to produce the curves shown in Figure 2.

Table 1. Calculations for Detector Measurement Spectra

Detector	No. of Calibration Filters	No. of Points for Curve Fit	Integrating Interval (μm)
UV	12	8	0.005
Blue	56	44	0.010
Red	28	9	0.010
IR	17	11	0.035

The air mass two measurement spectrum is shown in Figure 3, along with the air mass two solar spectrum according to Thekaekara [2]. To match the air mass two spectrum, given the spectral response $R(\lambda)$ of the four detectors, it is necessary to determine the best linear combination of the four spectra.

$$M(\lambda) = a_{UV}\, R_{UV}(\lambda) + a_{Blue}\, R_{Blue}(\lambda) + a_{Red}\, R_{Red}(\lambda) + a_{IR}\, R_{IR}(\lambda)$$

where, $M(\lambda)$ is the measurement spectrum

The best linear combination is determined by matching areas rather than attempting to match the curve point by point because of the irregular shape of the solar spectrum. The solar spectrum is divided into five wavelength ranges as shown in Figure 3, and the area under the curve is determined for each range. From the plots of the response spectra $R(\lambda)$ the areas are determined for each detector in the same wavelength ranges.

The areas are matched unsing the method of least square error. The result of the analysis is a set of four simultaneous equations in the four unknown multipliers (a_{UV}, a_{Blue}, a_{Red}, a_{IR}).

These equations are given in matrix form.

$$\underset{\sim}{S} = \underset{\sim}{D} \cdot \underset{\sim}{A} \qquad (4)$$

$$\underset{\sim}{S} = \begin{bmatrix} \sum_i S_i D_{UV,i} \\ \sum_i S_i D_{Blu,i} \\ \sum_i S_i D_{Red,i} \\ \sum_i S_i D_{IR,i} \end{bmatrix}$$

$$\underset{\sim}{D} = \begin{bmatrix} \sum_i D_{UV,i}^2 & \sum_i D_{UV,i} D_{Blu,i} & \sum_i D_{UV,i} D_{Red,i} & \sum_i D_{UV,i} D_{IR,i} \\ \sum_i D_{Blu,i} D_{UV,i} & \sum_i D_{Blu,i}^2 & \sum_i D_{Blu,i} D_{Red,i} & \sum_i D_{Blu,i} D_{IR,i} \\ \sum_i D_{Red,i} D_{UV,i} & \sum_i D_{Red,i} D_{Blu,i} & \sum_i D_{Red,i}^2 & \sum_i D_{Red,i} D_{IR,i} \\ \sum_i D_{IR,i} D_{UV,i} & \sum_i D_{IR,i} D_{Blu,i} & \sum_i D_{IR,i} D_{Red,i} & \sum_i D_{IR,i}^2 \end{bmatrix}$$

$$\underset{\sim}{A} = \begin{bmatrix} a_{UV} \\ a_{Blu} \\ a_{Red} \\ a_{IR} \end{bmatrix}$$

where, S_i - area, in the interval i, for the spectrum being matched

$D_{x,i}$ - area under detector response curve

Subscript i - indicates the wavelength interval

Table 2 gives the areas used for this matching procedure.

Table 2. Area (Energy) Distribution for the Four Detectors and the Air Mass Two Solar Spectrum

Wavelength Range (μm)	$D_{UV,i}$	$D_{Blue,i}$	$D_{Red,i}$	$D_{IR,i}$	Air Mass Two Solar Spectrum
.3-.4	2.71	0.23			1.71
.4-.6	0.22	10.62	4.61		16.14
.6-.9		0.72	23.51	0.42	22.9
.9-1.4			1.26	32.0	12.9
1.4-2.5				16.1	7.81

Notice that $\underset{\sim}{D}$ is independent of the spectrum to be fit, therefore to fit another spectrum it is only necessary to evaluate the column vector $\underset{\sim}{S}$. The inverse of $\underset{\sim}{D}$ was determined for the four detectors that are described here, so that the matching coefficients can be calculated from Figure 4 presents the air mass one solar spectrum and corresponding measurement spectrum.

$$\underset{\sim}{A} = \underset{\sim}{D}^{-1} \cdot \underset{\sim}{S} \tag{5}$$

$$\underset{\sim}{D}^{-1} = \begin{bmatrix} 1.371(10^{-1}) & -3.630(10^{-3}) & 1.775(10^{-4}) & -6.102(10^{-6}) \\ -3.631(10^{-3}) & 9.550(10^{-3}) & -1.091(10^{-3}) & 4.050(10^{-5}) \\ 1.775(10^{-4}) & -1.091(10^{-3}) & 1.870(10^{-3}) & -7.303(10^{-5}) \\ -6.103(10^{-6}) & 4.050(10^{-5}) & -7.303(10^{-5}) & 7.822(10^{-4}) \end{bmatrix} \tag{6}$$

Figure 4 presents the air mass one solar spectrum and corresponding measurement spectrum.

In order to calibrate the SSR to the desired spectrum, a reflectance standard is required. For this work a Kodak $BaSO_4$ paint [3] is used. Spectral reflectivity is shown in Figure 5 [4]. The calibration is accomplished as follows:

1. With the standard over the port the contribution of each detector to overall output should be,

$$\text{Reading}_x = \rho_x \, (a_x \, D_x / \sum_j a_j \, D_j) \tag{7}$$

where, x - UV, Blue, Red, IR

D_j - the total area under the response curve, $R(\lambda)$, for detector j

ρ_x - the reflectivity of the standard for detector x

2. Switch off all but one of the detectors and adjust the gain with the trimming potentiometer so that the appropriate reading is obtained. (switches and potentiometers are accessible through the front panel).

3. Repeat the adjustment for the other detectors. This completes the calibration and assures the attainment of the measurement spectrum.

Tables 3 and 4 summarize the detector weightings, etc. for the air mass one and air mass two measurement spectra.

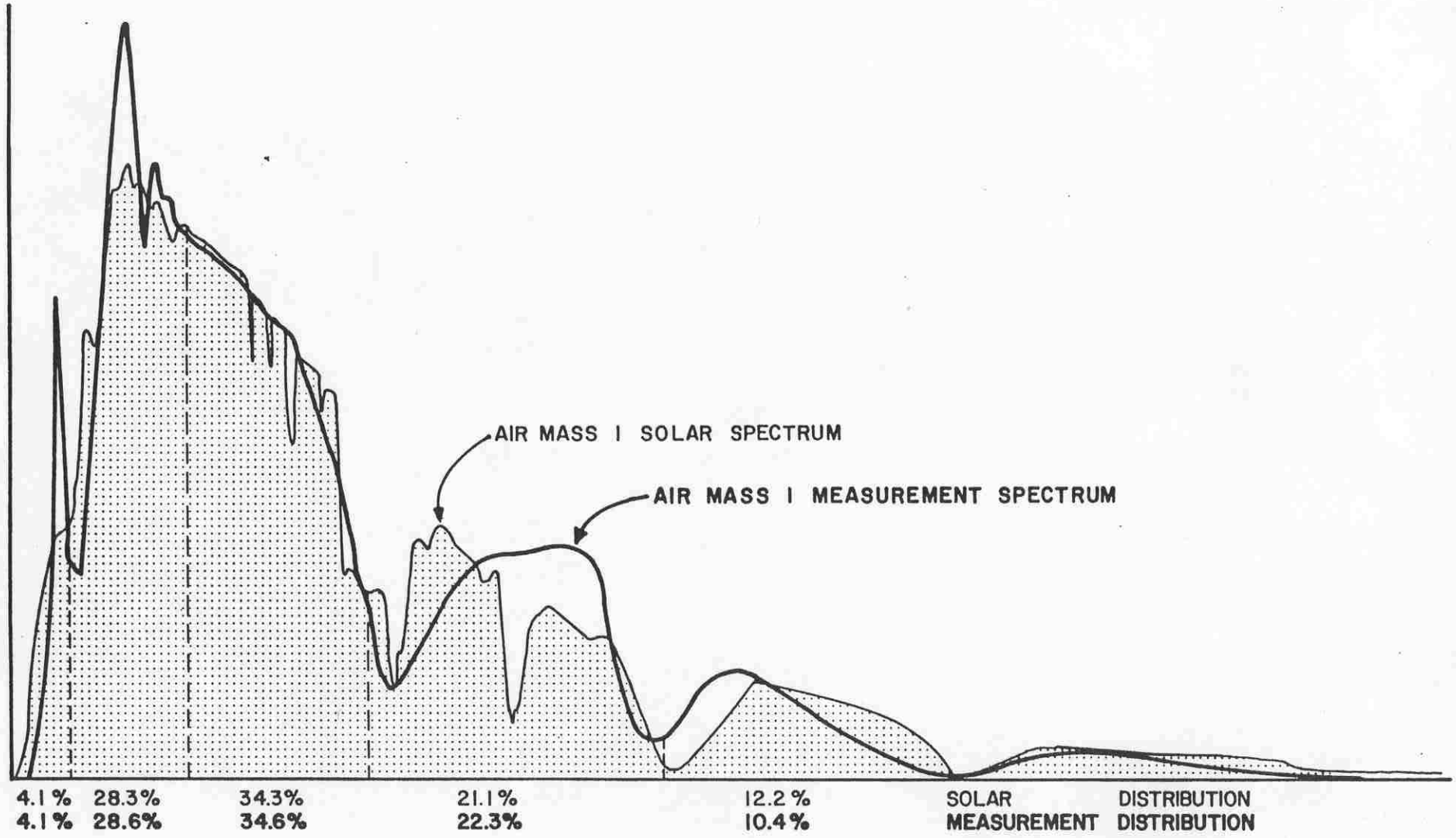

Figure 4. Comparison of the Air Mass 1 Solar Spectrum and the Air Mass 1 Measurement Spectrum

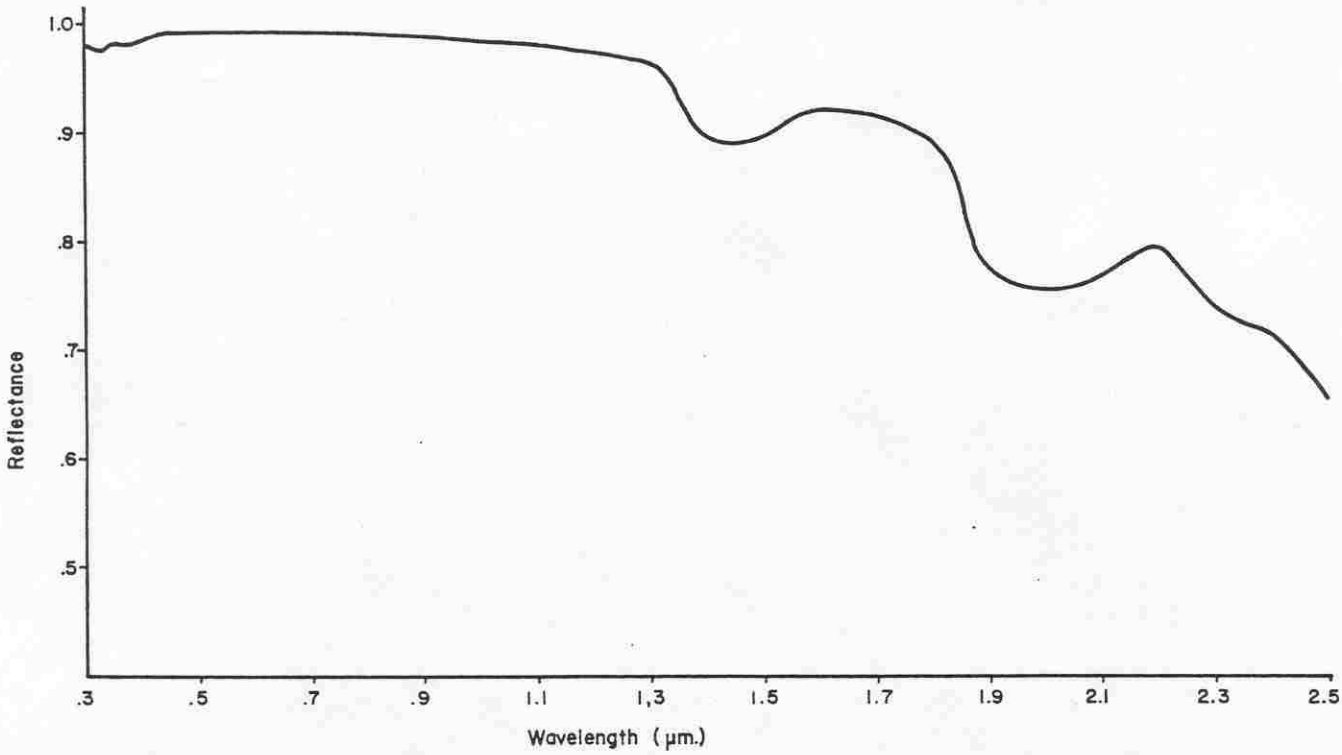

Figure 5. Spectral Reflectance of Barium Sulfate Standard

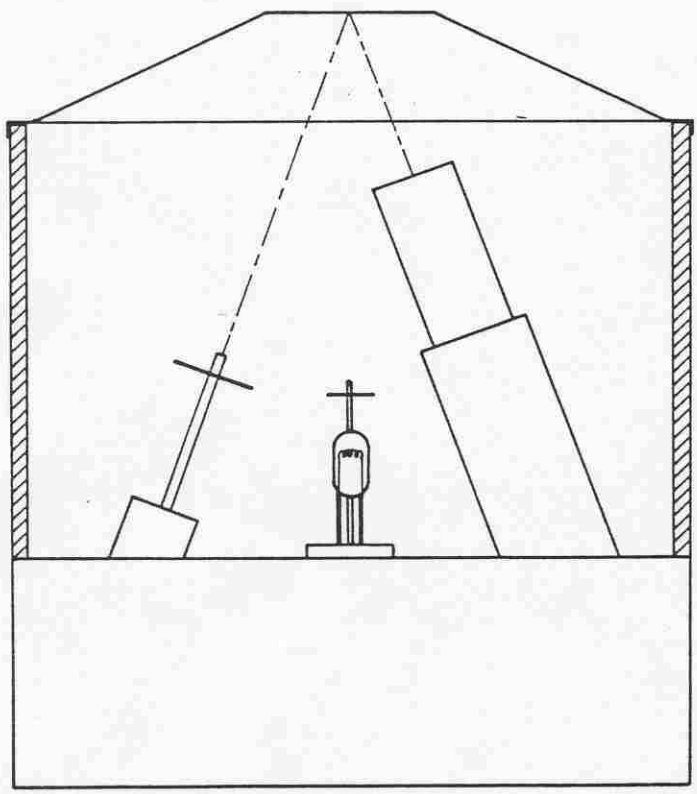

Figure 6. Cross Sectional View of Measurement Head

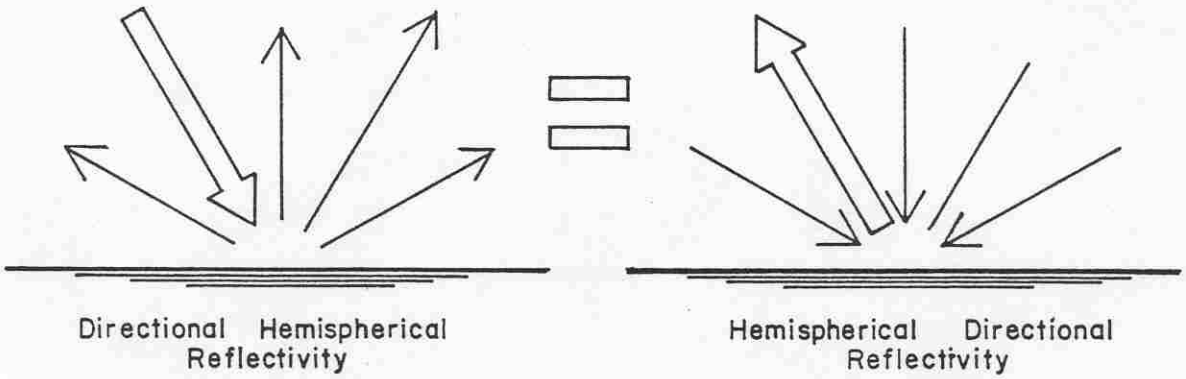

Figure 7. Reciprocity Relationship for Hemispherical-Directional and Directional-Hemispherical Reflectivities

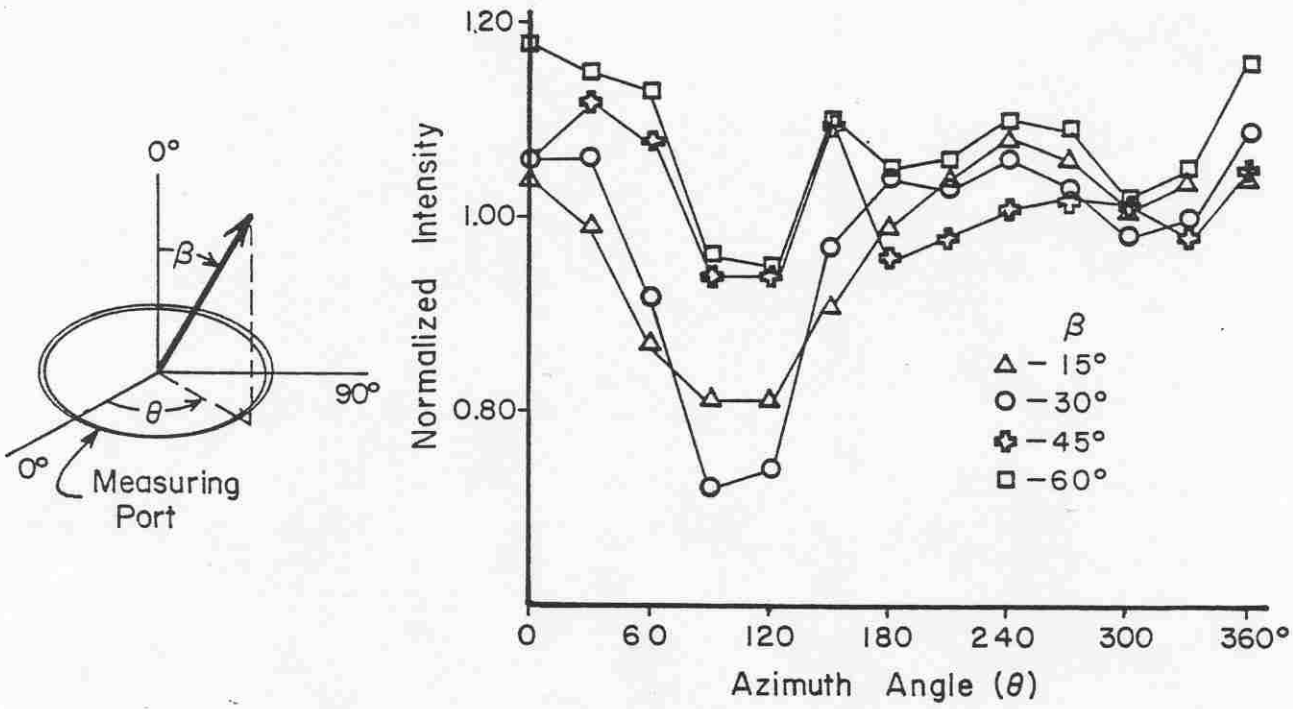

Figure 8. Distribution of Radiation Intensity at the Measurement Port

TABLE 3

Weighting and Detector Settings
for Air Mass Two Measurement Spectrum

Detector	Multiplier a_j	Detector Weighting	Reflectivity of $BaSO_4(\rho_x)$	$Reading_x$
UV	0.533	0.026	.981	0.025
Blue	1.121	0.21	.992	0.211
Red	0.930	0.45	.990	0.445
IR	0.391	0.31	.940	0.293
Total		1.00		0.974

TABLE 4

Weighting and Detector Settings
for Air Mass One Measurement Spectrum

Detector	Multiplier a_j	Detector Weighting	$Reading_x$
UV	0.79	0.039	.038
Blue	1.209	0.238	.236
Red	.818	0.410	.406
IR	.377	0.313	.294
Total		1.00	.974

EFFECT OF ANGULAR DISTRIBUTION OF INCIDENT ENERGY

The angular distribution as well as intensity and spectral distribution of incident energy affect the reflectivity measurement.

How the incident energy varies directionally and its significance is considered here. For most cases for surfaces of interest in solar energy collectors, or for building walls and roofs, errors caused by angular variation of the incident energy is small, typically less than 2% of reflectivity.

A sketch of the measurement head is given in Figure 6. The detectors are located in the collimator, and view the sample at 20° off normal to the sample surface. Barium sulfate paint on the walls of the chamber provides near diffuse illumination on the sample. The measured reflectivity will be the hemispherical-directional reflectivity. This is defined as the ratio of the radiation intensity reflected into a given direction to the incident intensity when the incident radiation is uniform in all directions, (i.e. diffuse).

By reciprocity this reflectivity is equivalent to the directional-hemispherical reflectivity which is defined as the reflectivity for energy incident from a given direction. Figure 7 illustrates reciprocity. For a solar application this would correspond to

the reflectivity of the surface for the beam component of the solar energy at 20° incidence.

Some measurement error is expected if the distribution of the energy exiting the measurement port is not perfectly diffuse. The variation of the radiation intensity with both the incident angle, β, and the azimuth angle θ is shown in Figure 8 for a prototype model. The minima at $\theta = 100°$ are caused by the opening in the collimator. The error, introduced by the fact that this is not perfectly uniform, is different for different samples since it depends on the distribution of reflected energy. Two factors minimize the error for most common materials.

First a barium sulfate paint is used to calibrate the reflectometer, as a standard for absolute reflectance. This coating is nearly diffuse, so for a diffuse sample (one that has near the same angular distribution of reflection as the standard) the error will be small. For a specular sample, however, most of the energy reflected into the collimator originates from the area of the chamber opposite the collimator. If the intensity in this area is higher or lower than the average intensity, the reflectivity of the specular sample will read high or low. This error is reduced in the SSR by adjusting the intensity coming from the specular direction. This is the purpose of the adjustable target shown in Figure 6.

Moving the target increases or decreases the relative amount of incident intensity in the specular direction. The adjustment is made by moving the target until the reading, with the red detector, for the diffuse Barium Sulfate sample and a front surface mirror are in the correct proportion.

The reflectivity of the front surface mirror was measured using the port of the measurement head as the light source, and a filtered silicon cell detector identical to the red detector used in the SSR.

By thus minimizing the errors for both diffuse and specular surfaces, the error is also small for most common surfaces since they exhibit primarily diffuse and specular components.

To estimate the measurement error for different surfaces, the incident energy distribution shown in Figure 9 was approximated as constant over ranges of azimuth angle.

The estimated error for a variety of surfaces for which bidirectional reflectivity data is available (reference [5], [6], [7], and [8]) is typically less than 2% of the reflectivity value. The exception is the rare case where the reflection is predominantly back into the direction of the incident beam, where the incident energy in the measurement head is a minimum due to the presence of the collimator. Figure 9 presents bidirectional reflectivity data for such a surface from reference [1]. Even for this surface, which is the worst case of backscatter that we found, the error is estimated to be less than 3% of the actual reflectivity.

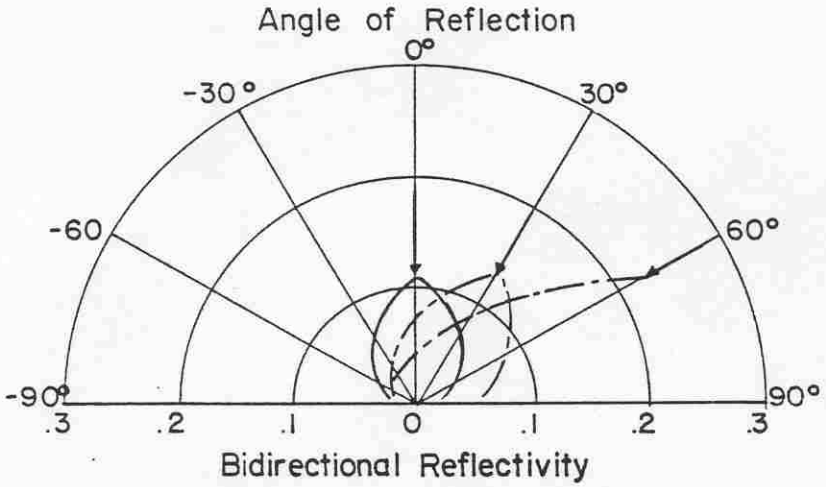

Figure 9. Bidirectional Reflectivity in the Plane of Incidence, from Orlova [1]

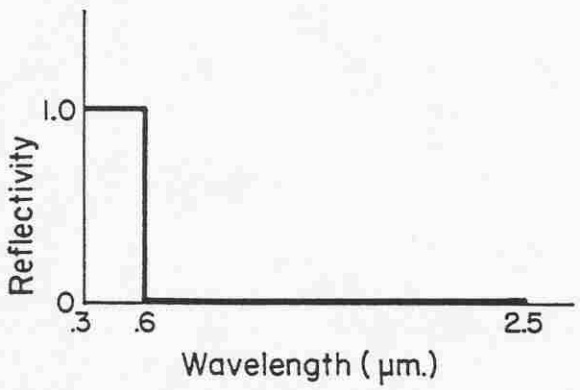

Figure 10. Spectral Reflectivity of a Surface Producing the Maximum Substitution Error

LAMP INTENSITY CONTROL

The intensity of the lamp is monitored with a silicon cell viewing the wall of the chamber. Lamp current is controlled to produce a constant output current from the silicon cell during the measurement period. In this way the control circuit maintains the lamp filament at a near constant temperature, and thereby prevents the measurement spectra and the weighting of the detectors from drifting. The filament resistance for different lamps are well matched so that it is only necessary to initially set the current to the lamp to reproduce the same filament temperature. Since for the tungsten halogen lamp the tungsten is prevented from evaporating on to the bulb, the spectral output of the lamp is relatively constant until just before the filament fails [9]. In addition, the tungsten lamp is rated at 1.17 amps with a 200 hr life, but the lamp is operated at 1.1 amps which should greatly extend the life of the bulb.

The silicon cell that controls the lamp views the side wall of the chamber, but does not view either the sample or the lamp directly. The purpose of controlling the light intensity from the chamber wall rather than directly from the lamp, is to minimize what is often called the substitution error. This error is caused by the fact that the incident energy on the sample depends on the reflectivity of the sample, since some of the energy reflected into the chamber is reflected back onto the sample. Since the chamber acts much like an integrating sphere, where due to multiple reflections the light intensity is uniform at every point, the intensity monitored on the wall of the chamber is indicative of the energy incident on the sample. By controlling this quantity at a constant value, however, the temperature of the filament must change slightly, i.e., slightly more current is required to keep the incident energy constant for a dark surface than a reflective surface. This will cause a shift in the weighting and very minor changes in the individual measurement spectra. In addition, if the sample is not spectrally flat the correction is only approximate, since the silicon cell responds primarily to energy in the Red and near IR.

To establish the remaining substitution error the change in the weighting for the maximum change in surface reflectivity must be determined. This is accomplished by measuring the lamp current with the $BaSO_4$ reflectance standard over the port and with the port open or a blackbody over the port. Then with the $BaSO_4$ sample on the port the lamp current is increased (a trimming potentiometer is available for this purpose) to read the same as it did with the port open. The change in weighting observed by this method is the largest possible variation. The largest error will be introduced for a surface with properties, as shown in Figure 10, where the reflectivity is low in the area of the silicon cell response, and high at shorter wavelengths. For the surface shown the actual reflectivity for the air mass two measurement spectrum is 0.29. The Reflectometer will indicate 0.30 due to the substitution error.

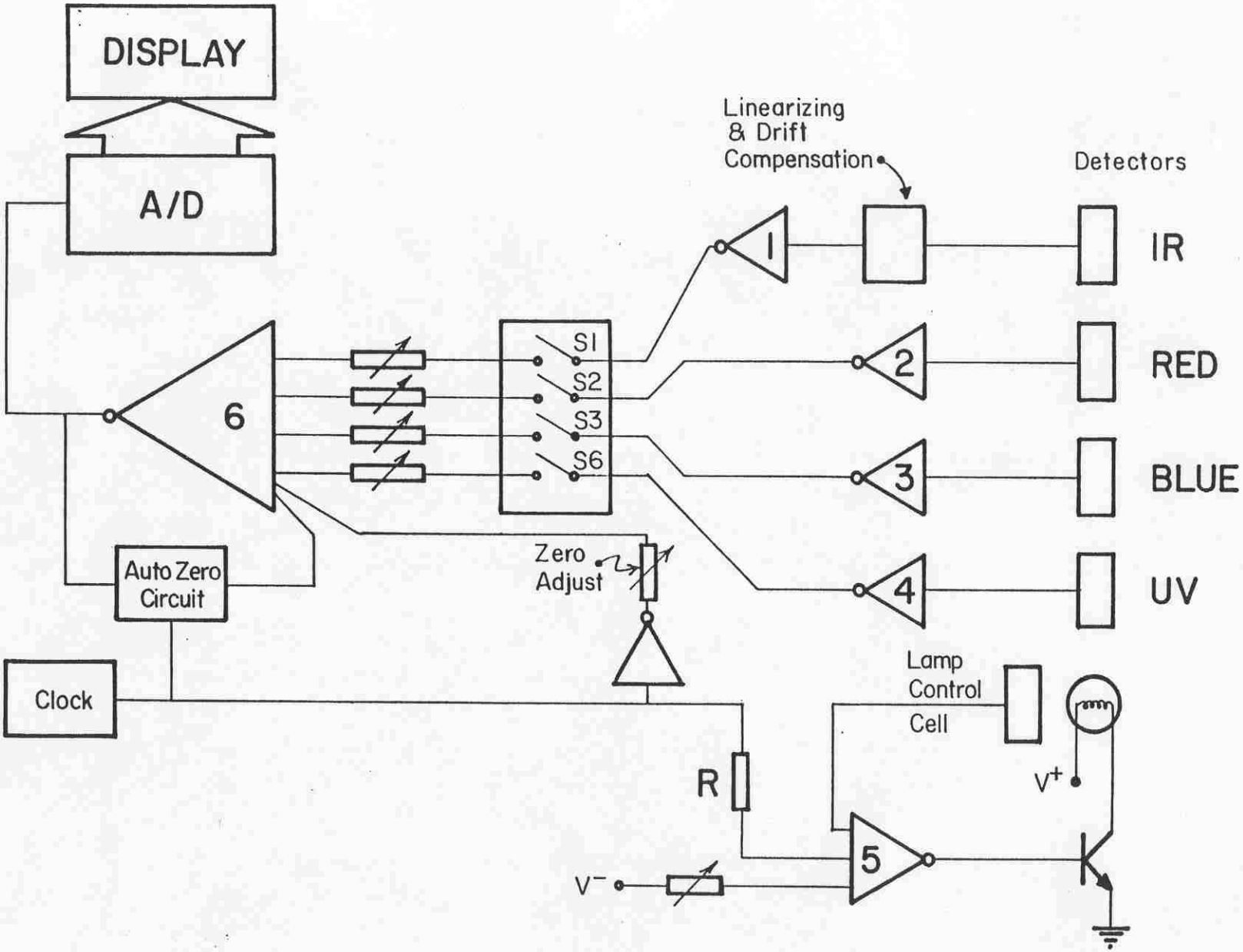

Figure 11. Operational Schematic of the Reflectometer

INSTRUMENT OPERATION

An operational schematic of the instrument is given in Figure 11. The switches and all of the trimmers shown in the figure are mounted on the circuit board and are accessible to the user through the removable panel on the front of the electronics housing. This enables the measurement spectrum to be adjusted as described above, by switching on the detectors one at a time. In addition, with these adjustments available to the user, the reflectivity of the sample for an individual detector measurement spectrum can be determined.

In order to attain the resolution and repeatability of the reflectometer without continual adjustment for offset drift, an automatic zeroing cycle (AZ), is incorporated in the electronics. Timing for the AZ cycle is established by a clock circuit that generates a logic output that is high for about 4 seconds once every 30 seconds. During the AZ period the current through resistor, R, forces the output of inverting amplifier 5 low, switching a transistor that turns off the lamp. While the lamp is off, the AZ circuit senses the output of amplifier 6 and drives the output to zero. During the measurement period the logic output is low, no current flows through R and the lamp intensity is controlled by the lamp control silicon cell.

An additional offset occurs due to the fact that the baffle system in the collimator cannot eliminate all of the stray light entering from the walls of the measurement head. Since the light is off during auto zero this offset is not nulled by the AZ circuit. This is the purpose of the additional input, to the summing amplifier, that is derived from the logic output. The inverted clock signal is high during the measurement period, producing a current that offsets the output due to the stray light, but producing no current during auto zero so that this additional input is not nulled out. A small hole in the removable panel provides access to this trimming potentiometer without removing the panel. Offset must be adjusted occasionally by using the blackbody cavity provided for this purpose.

Three optional outputs are available for use with recorders or automatic controls.

1. 0-10 volt analog output,
   V_{out} = 10 x sample reflectivity
2. Logic output that is normally low but high during auto zero
3. Logic output that is normally low but high if the circuit fails to auto zero during the 4 second period.

REFERENCES

[1] Orlova, N. S., Photometric Relief of the Lunar Surface, Astron. Z., Vol. 33 no. 1, pp. 93 - 100, 1956.

[2] Thekaekara, M. P., Supplement to the Proc. 20th Annual Meeting of Inst. for Environmental Sci., 21, "Data on Incident Solar Energy", 1974.

[3] Eastman White Reflectance Coating, Kodak publication No. JJ-32, 1976.

[4] Grum, F. and Luckey, G. W., "Optical Sphere Paint and a Working Standard of Reflectance", Applied Optics, Vol. 7, no. 11, p. 2289, 1968.

[5] Brandenburg, W. M. and Neu, J. T., "Unidirectional Reflectance of Imperfectly Diffuse Surfaces", J. Opt. Soc. Am., Vol. 56, no. 1, Jan. 1966.

[6] Middleton, W. E. Knowles and Mungall, A. G., "The Luminous Directional Reflectance of Snow", J. Opt. Soc. Am., Vol. 42, 8, Aug. 1952.

[7] Torrance, K. E. and Sparrow, E. M., "Biangular Reflectance of an Electric Nonconductor as a Function of Wavelength and Surface Roughness", J. Heat Transfer, Vol. 87, 2, May 1965.

[8] Birkebak, R. C. and Eckert, E. R. G., "Effects of Roughness of Metal Surfaces on Angular Distribution of Monochromatic Reflected Radiation", J. Heat Transfer, Vol. 87, 1, Feb. 1965.

[9] Halogen-Cycle Incandescent Lamps, General Electric, Publication no. 3-5257-R, April 1977.